Errichiello and Diarte Almada
Architectural Intelligence (2026) 5:16
https://doi.org/10.1007/s44223-026-00125-7

RESEARCH ARTICLE

Open Access

Experimental study of 3D printed biochar-mycelium composites via liquid deposition modeling for sustainable building components: compatibility, shrinkage control, structural integrity and prefabrication

Raffaele Errichiello[1*] and Julio C. Diarte Almada[1]

Abstract

What if building components could be 3D printed, grown, and welded together by living organisms? 3D printed mycelium-based composites (MBC) offer this potential but are limited by high shrinkage and low mechanical performance. This study pairs biochar, a stable, carbon-sequestering filler not yet tested with mycelium in additive manufacturing, with toolpaths inspired by brain-coral geometry designed to distribute oxygen-rich corridors and material-dense regions across the printed element, to support biological colonization and buildability. Eight empirical experiments address: biochar–mycelium compatibility, relationships between biomimetic toolpaths and bio-mechanical performance, and upscaling via segmented printing and bio-welding. Results show reduced vertical shrinkage (3–5%) under specific conditions, below typical lignocellulosic MBC values. Preliminary compressive tests suggest potential improvement, though sample size limits significance. A larger demonstrator was successfully printed and bio-welded, but dimensional stability still remained inconsistent. Future work will focus on water regulation for dimensional stability and mechanical analysis of gradients.

Keywords Mycelium-based composites, Biochar, 3D printing, Reaction–diffusion, Bio-welding

1 Introduction

The construction industry needs low-carbon, circular materials that can be shaped and produced efficiently. In this context, Mycelium-based composites (MBCs), produced when fungal mycelia colonize and bind lignocellulosic substrates, can sequester carbon and may offer foamlike, lightweight, and hydrophobic building elements with good thermal and acoustic insulation. Complementing these material approaches, 3D printing (3DP) of extrudable pastes via Liquid Deposition Modeling (LDM) can replace molds and reduce waste, enabling complex geometries. Yet, translating this promise into reliable building components presents challenges: 3D printable pastes must balance flowability with shape retention; water management is delicate; and shrinkage during growth and drying often compromises dimensional accuracy and structural integrity. In this work, we combine MBCs with biochar and reaction-diffusion inspired toolpaths, aiming to optimize oxygenation and stability of 3D-printed elements that can be prefabricated with low shrinkage and joined by bio-welding, a process in which mycelium's hyphae grow across the interface between more parts, fusing them into a continuous element

*Correspondence:
Raffaele Errichiello
raffaele.errichiello@umu.se
[1] Umeå School of Architecture, Umeå University, Östra Strandgatan 30 C, Umeå 903 33, Sweden

2 Literature background

2.1 Materials and rheology

Early material studies showed that MBCs can be prepared as printable pastes and deposited layer-by-layer, but also revealed laboratory-scale challenges: balancing flowability with rapid shape recovery, controlling water content, and limiting deformation during growth and drying (Bhardwaj et al., 2020). This has shifted attention toward rheological design, where particle size distributions, substrate chemistry, and binder/thickener strategies are tuned to achieve stable extrusion and interlayer adhesion while maintaining permeability for living systems (Mohseni et al., 2023; Özdemir et al., 2022).

2.2 Process and incubation workflows

As evidence of continuous progress in this area of research, several studies support larger fabrication adoption by addressing workflow constraints beyond the laboratory. For example, waste-based substrates and reduced sterility, or non-sterile approaches, are explored as routes for scalable fabrication, while nutrient calibration is treated as a key variable mediating both biological and structural behavior (Baharlou, 2025; Soh et al., 2023). Notably, Elsner et al. (2024) and Modanloo et al. (2021) emphasize incubation as an active fabrication stage that must be planned alongside printing to manage growth uniformity, interface bonding, and dimensional change.

2.3 Robotic deposition and assembly logics

At larger scales, research on robotic fabrication demonstrates that toolpath design and process control can be as impactful as formulation. These studies emphasize understanding critical parameters such as deposition rate, layer height, and path geometry to govern interlayer contact time, compaction, and moisture gradients, which affect bonding, warping, and cracking (Elsacker et al., 2022, 2023; Mohseni et al., 2023). Additionally, Chadha et al. (2023) and Schyck et al. (2024) claim the importance of defining fundamental steps such as printing, resting, incubating, drying, and the role of growth time to properly control the fabrication process.

Complementary hybrid robotic-analogue strategies appear as an alternative construction logic to enhance constructability and reduce dependency on paste rheology. Hybrid 3D printed formwork and manual assembly can define complex geometries that are later filled or colonized (Leschok & Dillenburger, 2022). Assembly is similarly reframed; instead of adding complementary materials to connect modular parts, bio-welding allows post-print mycelial growth to fuse interfaces between modules or bricks, turning segmentation into a scalable construction logic (Abdallah & Estévez, 2023; Modanloo et al., 2021).

2.4 Performance variability and standards

Beyond fabrication parameters control, reported mechanical performance evidence is promising but variable. Mechanical response depends strongly on fungal species, substrate granulometry, moisture content, anisotropy, and curing/drying protocols (Ghazvinian & Gürsoy, 2022; Rigobello & Ayres, 2022; Sharma & Sumbria, 2022). Recent studies probe species and process-dependent effects during fabrication and propose ways to enhance stiffness through engineered formulations, controlled growth, and hybrid approaches (Özdemir et al., 2025; Panjalipoursangari et al., 2025; Shen et al., 2024). Overall, the field is converging on the concept that geometry, fabrication, incubation, and drying must be co-designed rather than optimized sequentially, with clear needs for standardized printability metrics, predictive shrinkage models, and Life Cycle Assessments (LCA) (Madusanka et al., 2024; Rossi et al., 2022). Most recently, Bai et al. (2025) demonstrated shoot-deposition of MBCs at architectural scale, achieving compressive strengths up to 1.03 MPa with stable buildability over a 50-min window; the strongest reported value in the 3D-printed MBC corpus, though still well below the 17 MPa floor of low-density structural concrete.

2.5 Research gap and problem statement

Despite these advances, MBCs have mainly been adopted for packaging and insulation rather than structural elements, hypothetically due to persistent limitations related to shrinkage rates and mechanical performance. For example, MBCs incorporating lignocellulosic substrates exhibit shrinkage rates ranging from 9 to 20%, which affects geometric accuracy, in printed elements (Elsacker et al., 2019). Characterization studies report modest compressive strengths between 0.25 and 1.87 MPa and note deformation during drying, highlighting the need for improved formulations and processing strategies to reduce these issues (Aiduang et al., 2024; Mohanty et al., 2024). Consequently, this study explores how to reduce shrinkage and increase the mechanical performance of MBCs produced with 3DP by incorporating biochar in the substrate composition and introducing reaction–diffusion-inspired toolpaths.

Biochar, a carbon-rich material derived from the pyrolysis of organic waste, has attracted attention for its environmental benefits, including carbon sequestration, thermal insulation, and structural reinforcement in composite materials (Mohanty et al., 2024; Wang et al., 2025; Zhang et al., 2025). Biochar has been observed to mitigate shrinkage in cementitious composites, with Gupta

(2020) reporting a significant reduction in autogenous shrinkage when 5 wt% biochar was added to cement mortar. Despite these promising attributes, the compatibility of biochar and mycelium in composite materials remains largely unexplored, particularly regarding their application in 3DP. Furthermore, the community lacks a stress-aware design strategy that links material formulation to toolpaths that balance oxygenation and structural stability to achieve predictable growth, porosity, and stiffness within one print logic, especially at a larger scale.

2.6 Research questions

Based on the identified gaps, the hypothesis guiding this work is that biochar's low density, carbon composition, and stable structure may enhance mycelium growth, improve shape retention, and increase compressive strength, while reaction–diffusion-inspired toolpaths may balance oxygenation and structural integrity. Thus, this study addresses the following research questions:

a) How do biochar content and nutrient source influence extrudability, buildability, colonization consistency, and dimensional stability in MBCs for 3D printing via LDM?
b) Can reaction–diffusion-inspired toolpaths contribute to balancing biological and mechanical performance during printing, growing, and drying?
c) How can the printing toolpath be parameterized and the fabrication workflow adapted to preserve biological and mechanical performance characteristics when scaling up from small specimens to building components?

2.7 Paper organization and contribution

This paper includes preliminary findings presented at the International *Conference on Computational Design and Robotic Fabrication (CDRF) 2025* (Errichiello & Diarte Almada, 2025). Those findings correspond to the first experimental set reported here (Tests 1–4), which focuses on material compatibility and initial geometry and toolpath definitions. The conference paper was substantially extended in this manuscript by adding a second experimental set (Tests 5–8) in which geometry definitions were fine-tuned, material ratios refined, small specimens scaled to a demonstrator to test overhang limits, bio-welding of modular parts introduced, and mechanical performance benchmarked. The paper contributes a workflow that couples biochar-mycelium formulations with reaction–diffusion inspired toolpaths, traced from specimens to a bio-welded demonstrator and documented with preliminary mechanical benchmarks and implementation parameters.

Beyond materials and fabrication, this study is situated within a new biobased material paradigm where architecture is reshaped by the embedded lifespans of living, site-specific composites (Thomsen & Tamke, 2022). MBCs are not simply substitute materials to be inserted into existing construction typologies; their biological nature and foam-like mechanical behavior suggest compression-only, self-supporting geometries, calling for a tectonic rethinking of how elements are shaped, joined, and maintained. The present paper contributes to the material and process foundation on which these architectural visions depend. Without predictable formulations, controlled shrinkage, and reliable prefabrication processes, larger-scale architectural applications remain speculative.

3 Methods

The experimental design follows an empirical, iterative optimization process. Since no standardized protocol exists for biochar-mycelium composites fabricated via LDM, each test was adapted to address questions emerging from the previous one, and multiple variables were varied in parallel where strict single-variable isolation was not practicable. Two sequential sets (Tests 1–4; Tests 5–8) (Fig. 1) were planned around basic working hypotheses, and the sequence advanced only after meeting predefined acceptance criteria: clean extrusion, uniform colonization with low contamination, and basic dimensional stability. The eight empirical experiments were selected as the minimal set to answer the research questions while progressively controlling material, geometry, and assembly variables.

The first set (Tests 1–4) was guided by the hypothesis that biochar would improve shape retention in the wet state and increase compressive strength in the dry state, while the reaction–diffusion-inspired toolpath would support mycelial growth by managing oxygenation, moisture, and buildability. The goal was to establish feasible material combinations and toolpath fundamentals. In Test 1, biochar-mycelium mixes were screened for compatibility and printability in Ø50 × 50 mm height cylinders; then in Test 2, the impact of nutrient sources was visually compared to minimize contamination. Next, in Test 3, the focus was shifted from material to geometry, and a reaction–diffusion-inspired toolpath was integrated to create a porous structure to promote oxygenation while allowing buildability. The hypothesis was that, at certain points along the toolpath, extruding the material so close to merge with the previous extrusions would improve print stability. In Test 4, wood fibers

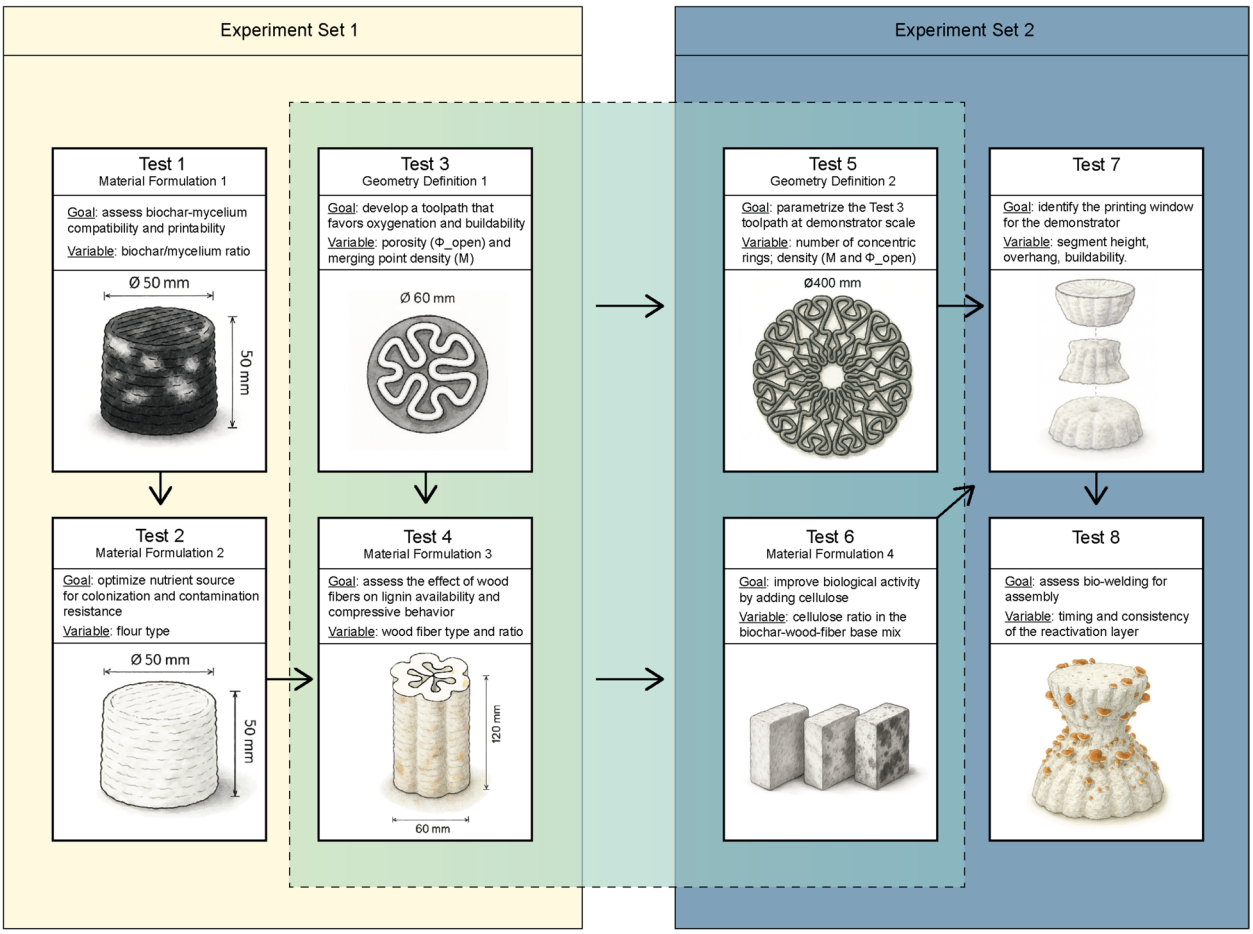

Fig. 1 Methods overview: two sequential experiment sets and their convergence. Set 1 (Tests 1–4) establishes formulation and toolpaths in specimens; Set 2 (Tests 5–8) upscales and produces a demonstrator

were added as a lignin source, and the sample's dimensions were changed to Ø60×120 mm to test compressive behavior.

In the second set (Tests 5–8), the hypothesis was that the geometry and material behavior observed in specimens could be preserved at demonstrator scale, and that the resulting segments could be joined into a single element via bio-welding. The geometry rules were upscaled to a Ø400×400 mm height demonstrator. For this, in Test 5, the pattern's generative logic used in Test 3 and Test 4 was parametrized to hold 2 design constants: merging point density (M) and porosity (Φ_open). In this study, a merging point (M) is a place where the toolpath overlaps, connecting the extruded material, while porosity (Φ_open) refers to the relation between filled and void spaces in the samples or demonstrator.

Next, in Test 6, the mix was refined with cellulose to provide a more easily degradable substrate for the fungus. The printability window was mapped for curved overhangs in Test 7, and a segmentation strategy was developed to test the composite's fresh-state limits. In Test 8, the 3D printed segments were merged through bio-welding using a thin layer of fresh composite mix to reactivate the mycelium hyphae and join the parts; the element was then air-dried. The arrows in Fig. 1 trace how insights propagated, geometry from Test 3 to Test 5, formulation from Test 4 to Test 6, and so on.

3.1 Experimental set 1—samples (Test 1, 2, 3, and 4)

This study utilized a range of biobased and commercially available materials to formulate biochar-mycelium composites for 3D printing. The *biochar* sample was sourced from the *Swedish Energy Industry*; however, its precise feedstock and pyrolysis conditions remain unknown. The primary objective was to evaluate its functional performance in combination with mycelium, evaluating the results based on experimental observations, without detailed material characterizations. The mycelium strain used was *M9726*

Ganoderma lucidum, provided in seed spawn from *mycelia.be*. This strain was used due to its rapid mycelium development and self-healing properties (Elsacker et al., 2023). We then incorporated 2 types of wood fibers: *fine sawdust* collected from the university's wood shop, with unknown wood species and possible prior treatments, and *untreated wood fiber pellets* supplied by the *Research Institutes of Sweden* (*RI.SE*) in Mölndal, whose compositional properties were also unknown. To enhance mycelium development, 3 types of flour were sourced (*tapioca*, *full grain*, and *rice flour*) from a local food store. Additionally, *xanthan gum* and *glycerol*, needed as binders and plasticizers, were bought from local commercial suppliers.

The experimental procedures, relative to 3DP, were carried out using a *WASP 40100 LDM* 3D printer equipped with a *manual-feeding extruder* and a 6 mm nozzle. Biochar and wood fibers were sterilized using a *GETINGE HS Lab Steam Sterilizer*, while kitchen utensils were used for pasteurization by boiling.

The growing phases were staged using a custom-made fermentation chamber measuring 1200×1200×800 mm, covered with transparent plastic film and equipped with a thermostat, heating mats, and a humidifier. The digital modeling and toolpath generation of printed samples were prepared with *Rhinoceros 3D* and *Grasshopper*. To evaluate the potential of biochar-mycelium composites for 3D printing, four tests were conducted, each addressing different aspects of material formulation, printability, and structural performance. Table 1 summarizes the goals, experiments' setup, and data collection methods for tests 1–4.

3.2 Experimental set 2 – prototype (Test 5, 6, 7, and 8)

Set 2 extended the insights from Set 1 to a Ø400×400 mm height prototype. Test 5 increased the complexity of the geometry developed in Test 3 (from 1–3 rings of points cloud to 4–5 interwoven rings), seeking to evenly distribute merging points and moisture chambers and to investigate printing performance under overhang conditions. Also, the toolpath was upscaled from a 6 mm to an 8 mm nozzle and kept 2 constants across height and curvature: merging point (M) and porosity (Φ_open). Test 6 refined the material formulation from Test 4, adding cellulose from recycled cardboard pulp to accelerate fungal access to a lignocellulose source while reducing biochar content. Test 7 ran printing trials to frame the printing parameters before producing the prototype, as 3 segments (~150 mm high, each) and growing them. Test 8 evaluated assembly with a thin layer of fresh composite paste between segments, followed by a short growth phase of 7 days and extended air-drying for at least 28 days. Table 2 summarizes the experimental Set 2 specific goals and setup.

4 Results

The experimental tests provided specific observations regarding printability, mycelium growth, structural integrity, and contamination issues associated with the biochar-mycelium composites.

4.1 Experimental set 1: compatibility, nutrient sources, and buildability

In Test 1 (Fig. 2), sample 1.1 exhibited extruder clogging in all replicas, ¾ replicas showed no clogging in 1.2, while all replicas in 1.3 and 1.4 printed without clogging. While sample 1.4, with higher biochar content, faced difficulties in extrusion consistency in ½ replicas, resulting in uneven and brittle extrusion. Despite the clogging episodes, sufficient material from sample 1.1 could be consolidated into the four cylindrical specimens used for compressive tests. Rapid moisture loss and contamination were observed after one week in all samples.

Test 2 (Fig. 3) investigated the role of flour type in optimizing mycelium growth and maintaining antimicrobial resistance. Firstly, *tapioca flour* (Fig. 3–1.3) resulted in poor mycelium growth and evident contamination. Next, *wheat flour* (Fig. 3–2.3) had more uniform growth, with less contamination compared to *tapioca flour*. Finally, *rice flour* (Fig. 3–3.3) provided optimal results with consistent mycelium growth and no visible contamination.

In Test 3 (Fig. 4), geometry optimization informed by reaction–diffusion patterns enhanced oxygenation of the composite and structural integrity compared to the previous sample design. Figure 4 illustrates a comparative evaluation of 12 different design iterations, analyzing the relationship between the material´s merging points along the 3D printing paths and the porosity rate. Design iterations G3 and G7 were selected for further prototyping in Test 4 (Fig. 5) for their balanced relation of porosity and number of merging points.

Test 4 evaluated the inclusion of wood fibers to enhance lignin content and structural behavior of the composites (Fig. 5). Geometry G3 in sample 3.A and 3.B kept structural integrity. Sample 3.A, with slight over-extrusion, favored buildability. Samples 3.B, 3.C, and 3.E required adjustments in water content for successful extrusion. Mycelial growth was visually uniform across all Test 4 samples after 14 days of incubation; samples containing workshop sawdust (3.A-3.C) exhibited the densest and most continuous surface colonization, as documented in Fig. 5. Sample 3.E was significantly contaminated. Higher wood fiber content promoted *fruiting bodies* and *melanin* development, which is not preferable for the research's goals.

In addition to growth and printability, preliminary compressive tests were conducted on selected samples from Test 1, Test 2, and Test 4 to assess their structural

Table 1 Set 1—Research tests goals, study set-up, and data collection methods

Goals	Experiments' set-up	Data collection
Test 1: Assess the compatibility of biochar and mycelium in different formulations for 3D printing and evaluate printability	4 biochar-mycelium formulations were prepared, stored in a fermentation box for 48 h, and 3D printed into small cylinders (50 mm diameter, 50 mm height). Each formulation was printed in 4 replicas for comparability. Samples were then evaluated for printability and initial mycelium growth	Printability assessment, photographic documentation of samples over 2 weeks, weight monitoring of formulation 1.3 to track water content
Test 2: Investigate the influence of different nutritional sources on mycelium growth	The most promising formulation from Test 1 (1.3) was modified by replacing tapioca flour with whole grain wheat flour (sample 2.3) and rice flour (sample 3.3). The new formulations were 3D printed into cylinders (50 mm diameter, 50 mm height), with 4 replicas for each formulation, to monitor their mycelium development	Mycelium growth was documented photographically every 24 h over 2 weeks
Test 3: Develop geometries that enhance oxygenation and structural integrity, suitable for compressive tests	New geometries were designed to improve oxygenation and mycelial growth. The geometries were informed by reaction–diffusion patterns observed in brain corals, which use this geometry to promote fluid circulation and nutrient exchange. 12 variations (G1-G12) were generated using *Grasshopper* and *Rhinoceros 3D*. G3 and G7 were selected for their balance among *porosity* and path´s *merging points*	Structural and porosity characteristics of the geometries were analyzed. Evaluation was based on visual differences in *porosity* percentage and number of *merging points* among the variations
Test 4: Enhance composite tensile resistance and lignin content by integrating wood fibers into biochar-mycelium formulations	Biochar and wood fibers were sterilized using an autoclave (120 °C, 15 min) and mixed in 5 formulations (3.A—3.E). After 14 days of initial growth at 24 °C, the samples were 3D printed into cylinders (60 mm diameter, 120 mm height) using 2 printing paths (G3, G7). Printed samples were kept fermenting at 24 °C on 90 mm petri dishes covered with 600 ml plastic cups for 2 weeks. Each combination of geometry (G3, G7) and material formulation (3.A-3.E) was printed once	Growth patterns and moisture content were documented every 48 h. On day 7th and 14th, contamination, mycelium growth consistency and shrinkage across samples were marked

Table 2 Set 2—Research tests goals, study setup, and data collection methods

Goals	Experiments' set-up	Data collection
Test 5: Refine and parametrize the printing path's geometry to distribute merging points (M) and porosity (Φ_open) more evenly, while keeping them proportioned across sections	Building on Test 3, the geometry was adapted on a Ø400 mm dodecagon through concentric rings scaled by φ. The point clouds were divided, phase-shifted, and interwoven into a single path. The geometry was adapted to an 8 mm nozzle and 4 mm layer height: path except to blend at *merging points*; *moisture wells* and *oxygens corridors* regulate the mycelium growth. A *central* through-ventilation *cavity* and narrow *densification belts* were included for handling and airflow control	Measurements of Φ_open and M at base/waist/top sections; 3 horizontal sections were compared to G3 and G7 paths from Test 3; Vertical sections were used to check the airflows generated along the Z axis
Test 6: Improve fungal growth and balance biochar content by adding cellulose; screen 3 formulations for mycelial compatibility and material viscosity before printing	A cellulose (cardboard pulp) component was added to the biochar-wood-fiber mixture from Test 4 (*Sample 3.A*). 3 ratios were prepared, mixed under the same hygiene protocol, and cast into 100 × 100 × 30 mm blocks using plastic formworks. The samples were incubated for 14 days at 24 °C in darkness to promote colonization	Samples were photographed after incubation and dehydration and assessed them for colonization uniformity, contamination, surface cohesion and shrinkage
Test 7: Establish a printing window for the selected mix and define the segments' height relative to the prototype' s curvature; verify fresh-state dimensional stability and overhang achievability	A first attempt tested the possibility of producing a single piece element of 400 mm height; a second attempt investigated a practical strategy to section the prototype into 3 elements with a height of around 150 mm, drawing from the specimens produced during Test 4 (120 mm height). 3 segments (≈ base 112 mm, middle 124 mm, top 164 mm) were selected according to their curvature. Each segment was printed and grown 14 days at 24–26 °C in darkness	A segmentation diagram shows curvature zones and cutting planes. Printed elements were analyzed through photographic documentation, and their diameters and heights were checked after 14 days. Then they were partially dried at room temperature for 7 days
Test 8: Evaluate assembly via a bio-welding after partial drying to assess procedural feasibility before extended air-drying	A thin layer of fresh mycelium paste (same composition) was applied to matching faces, the segments were aligned, keeping the central corridor open. The assembly grew 7 days (24 °C, darkness) and then air-dried for more than 28 days at room temperature	Photographic documentation monitored the bio-welding, contamination, and dimensional stability after 7 and more than 28 days

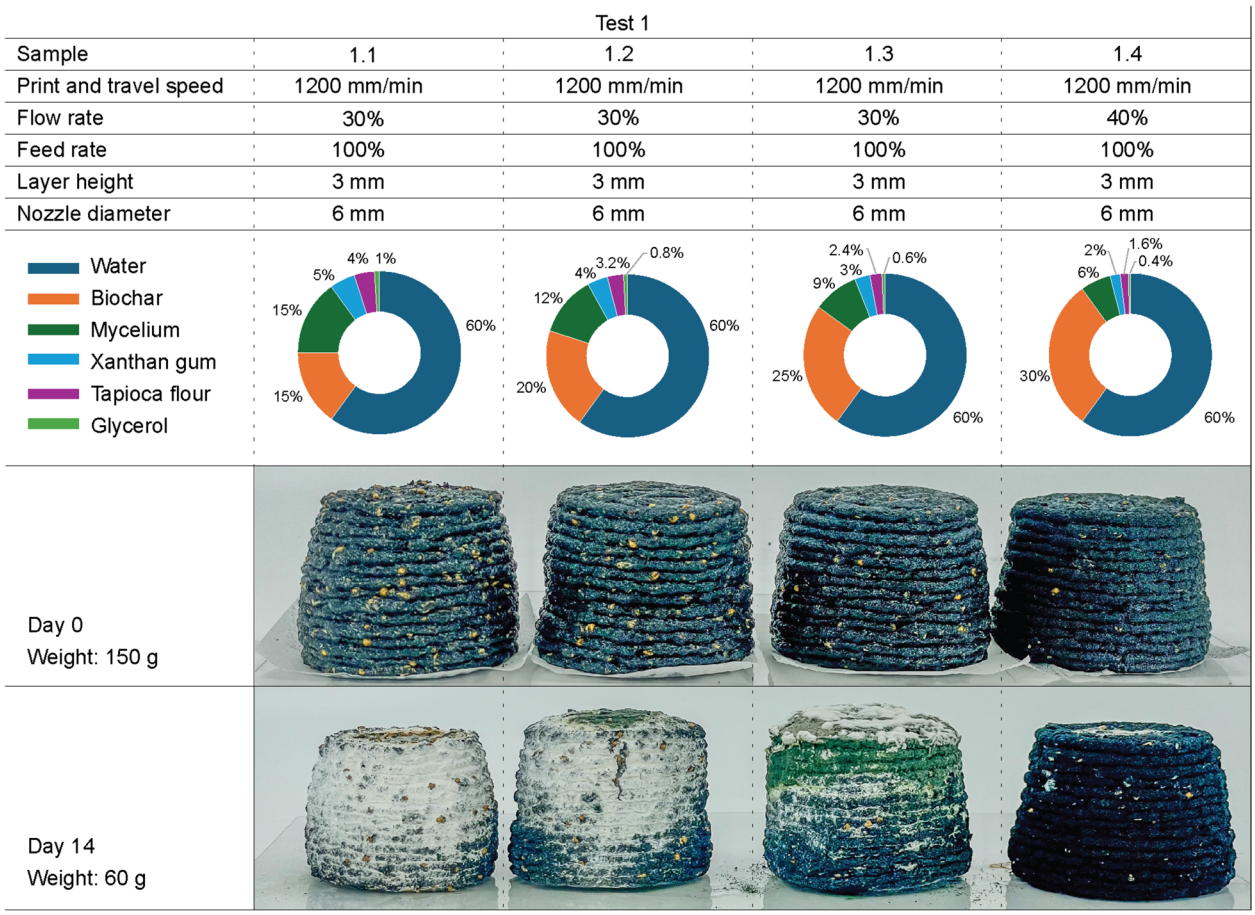

Fig. 2 Samples composition, printing parameters, and growing documentation for 14 days during Test 1 (**a**) and Test 1 (**b**)

performance. These tests measured peak force, stroke, strain, compressive strength, and elastic modulus across various geometries and formulations. Results are summarized in Table 3, which presents the mechanical properties of the most representative samples, including averages for 1.1 and 3.3, and all tested 3.A-E composites.

4.2 Experimental set 2: parameterized toolpath, fungal growth, upscaling, and assembly

In Test 5 (Fig. 6), the reaction–diffusion-inspired design used for the samples of Ø60 × 120 mm height (Fig. 6-G3, G7) was upscaled to test the fabrication of a Ø400 × 400 mm height prototype (Fig. 6-Gx, Gy, Gz). The 2 parameters defined in Test 3 were preserved: merging point density (M) and porosity (Φ_open), this time using an 8 mm nozzle. The printing path was generated by weaving the points along concentric rings (e.g., 4 rings for Gy and 5 rings for Gx and Gz).

To provide an easily degradable lignin source, in Test 6 (Fig. 7), 3 mixes integrating cellulose in different ratios were screened (cardboard pulp added to 3.A mixture from Test 4) through 100 × 100 × 30 mm samples incubated 14 days at 24 °C and assessed for colonization uniformity, surface cohesion, visible contamination, and shrinkage.

Test 7 (Fig. 8) focused on the fabrication of a larger demonstrator. Firstly, a 1:5 scale model was 3D printed to verify that the path was printing as expected and that the central cavities would remain open to air (Fig. 8-a). These phases also checked the double-curved shape and the relative overhangs; these were designed considering the constant curvature of a sphere to control the degree of curvature of the overhangs, keeping them around less than 45 degrees (Fig. 8-b). Next, the demonstrator was 3D printed at full scale in one run. An initial attempt investigated this hypothesis, but the samples were collapsing due to the overweight and weakness of the wet composite. To fix this, the prototype was segmented into 3 parts along the Z axis (S1 = 112 mm base, S2 = 124 mm middle/waist, S3 = 164 mm top), managing wet mass and unsupported spans while keeping overhangs within ≤ 45°. These segments are shown in

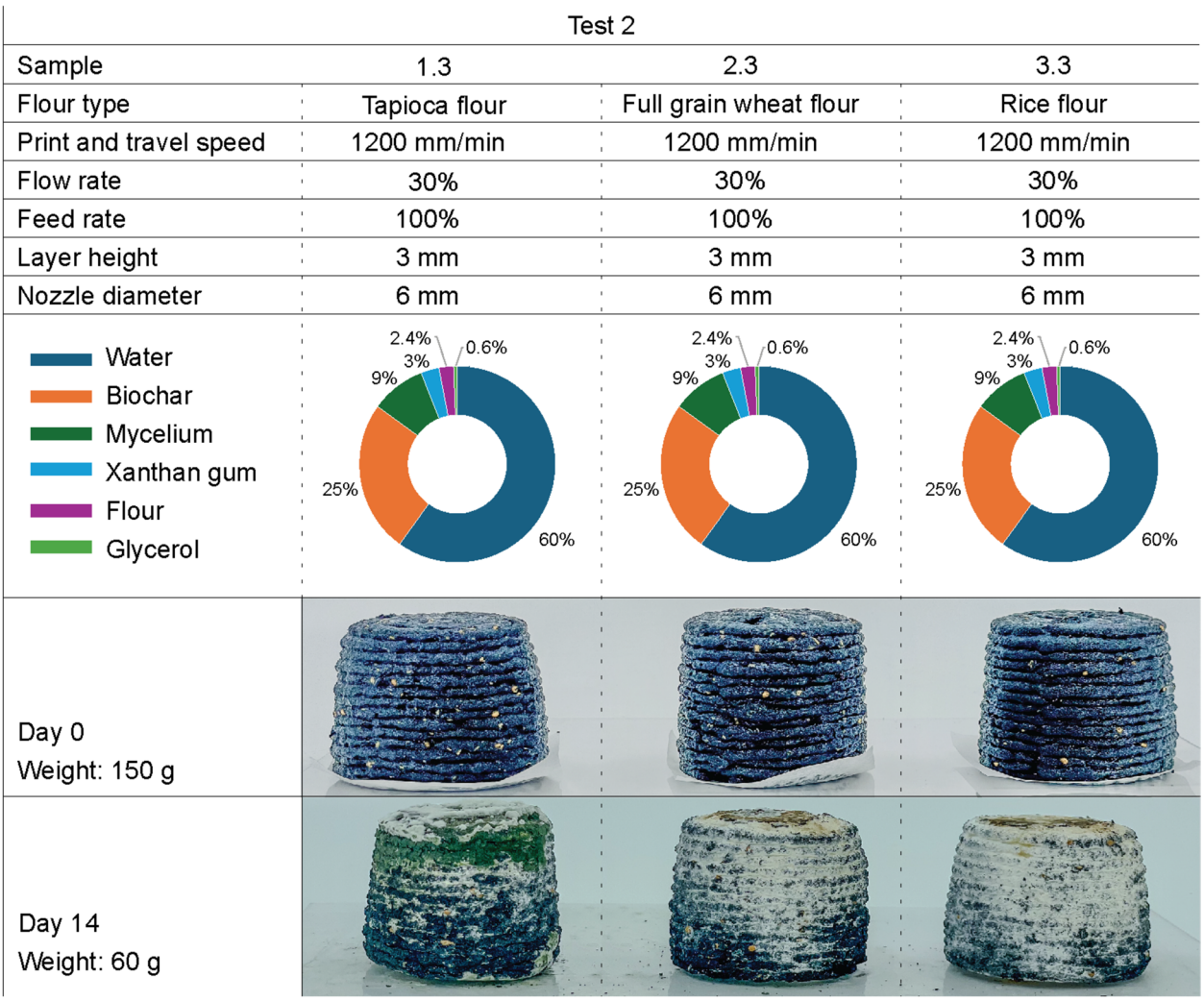

Fig. 3 Samples composition, printing parameters, and growing documentation for 14 days during Test 2 (**a**) and Test 2 (**b**)

Fig. 8-b, together with prototype dimensions and overhangs in the digital model.

After the mycelium growth and after 7 days of dehydration at room temperature, the segments were assembled (Test 8).

Before joining, the mating faces were re-activated with a thin layer of fresh composite, intentionally keeping the central corridor open to air. Within the first week, mycelium's hyphae constantly appeared, thickening into a continuous skin.

5 Discussion

This experimental study explored biochar-mycelium composites for 3D Printing via LDM, highlighting their potential while identifying significant limitations. The most significant challenges identified were printability, moisture regulation, and contamination control.

5.1 Biochar-mycelium compatibility, formulation, and contamination control

Research question (a) asked whether mycelium and biochar are compatible in 3D printable pastes and what mix supports extrudability, buildability, and consistent growth. The results from Tests 1, 2, 4, and 6 collectively indicate that biochar and mycelium are compatible within a defined formulation window, with rice flour emerging as the preferred nutrient source for uniform colonization and contamination resistance.

Test 1 investigated the compatibility among mycelium and biochar and printability parameters, evaluating 4 different ratios of the 2 main components and identifying that samples 1.3 and 1.4 had better printability and buildability. This was probably due to their lowered mycelium content from 15–12 wt% (Samples 1.1 and 1.2) to 9–6 wt% (Samples 1.3 and 1.4) while biochar content increased from 15–20 wt% to 20–25 wt%, respectively.

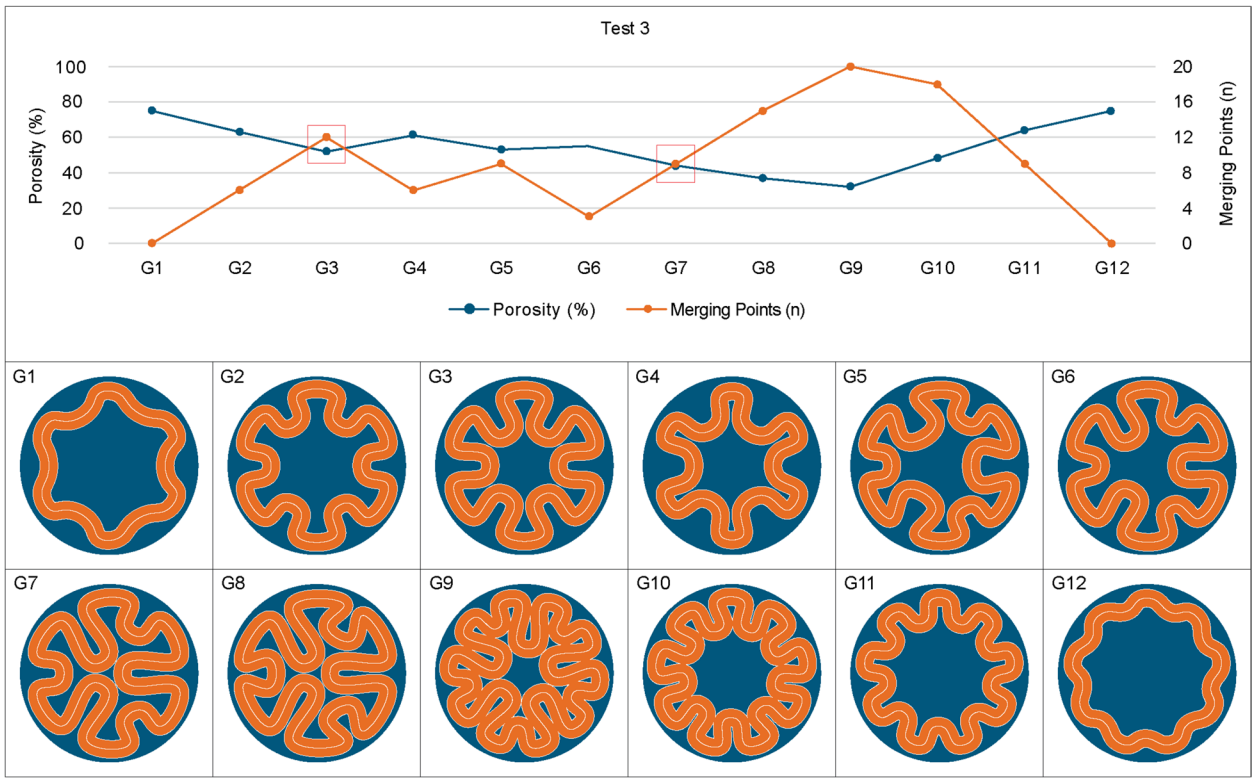

Fig. 4 Comparative geometries evaluation for Test 3

This aligns with Mohanty et al. (2024), who identified 20–25 wt% as the optimal content for biocarbon in composite materials before particle agglomeration begins to degrade properties. The improvement, in printability at lower mycelium content is also consistent with the challenges reported by Bhardwaj et al. (2020), whose MBC required psyllium husk binders to prevent phase segregation at high moisture and spawn ratio, and with Elsacker et al. (2022), who found that high-viscosity MBCs may lead to extruder clogging. In our formulations, the granular biochar appears to fulfill part of the structural role that gelling agents have in other formulations, contributing to shape retention without the viscosity peaks that cause nozzle jam.

Test 2 highlighted the critical role of flour type as a nutrient. As shown in Fig. 3, visual observation of sample 3.3 (*rice flour*) suggests improved mycelial growth and antimicrobial resistance compared to samples 1.3 (*tapioca)* and 2.3 (*wheat flour).* The dominant nutrient sources in the literature are wheat-based: Mohseni et al. (2023) used wheat bran with waste cardboard, Bhardwaj et al. (2020) relied on wheat flour, and Soh et al. (2023) employed malt extract and peptone. None of these studies reported antimicrobial benefits from their nutrient choice. Baharlou (2025) explicitly framed nutrient calibration as a key variable mediating both biological and structural behavior, finding that 10 wt% malt extract agar optimally supported aerial, surface, and penetrative mycelium growth in soil-based inks. Our observation that rice flour could have enhanced contamination resistance suggests that starch type may influence antimicrobial outcomes through mechanisms not yet explored in the literature.

Moreover, while Mohseni et al. (2023) reported substrates autoclaved at 121 °C for 40 min, all mixing in a laminar airflow biosafety hood, and 70% ethanol on all surfaces, Soh et al. (2023) achieved open-air, non-sterile printing with a contamination rate below 10% by accelerating mycelium colonization through nutrient supplements. Our approach occupies a middle ground: we sterilized substrates but did not require sterile-room conditions for printing and handling, relying instead on the nutritional source and controlled humidity to limit contamination. Ongoing research collaboration with the Molecular Biology Department at Umeå University on this project aims to enhance the composite´s antimicrobial properties by targeting the types of contaminants present in the components used as substrate to define a strategy for contamination mitigation.

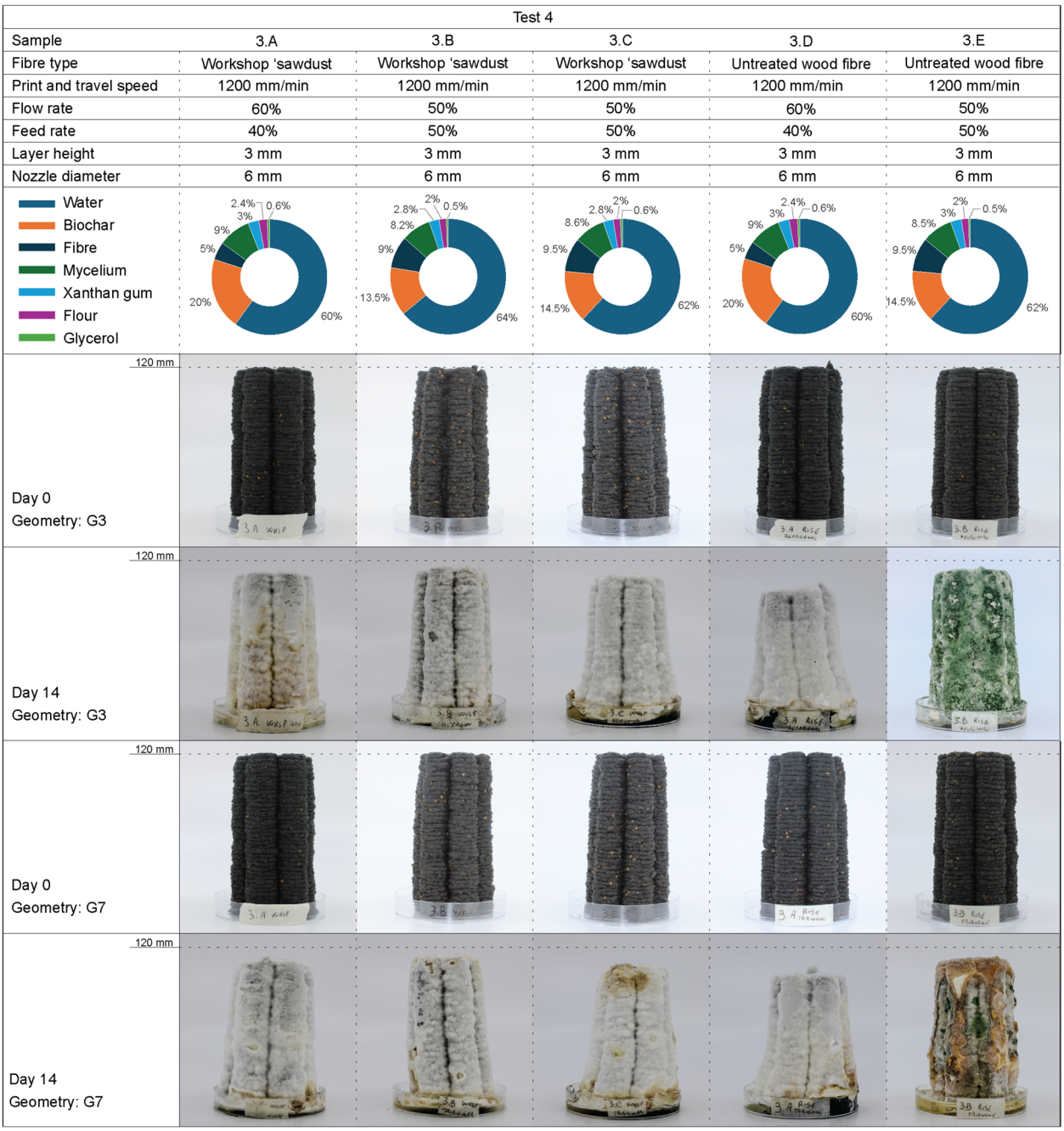

Fig. 5 Test 4 samples composition, printing parameters, and growing documentation for 14 days

These initial tests revealed that inconsistent humidity significantly impacted mycelium growth, leading to uneven colonization. By adjusting the size of the fermentation chamber in Test 4, stable humidity conditions were successfully maintained, losing only 2–4% of water content after one week, and 6–8% after 2 weeks, mitigating this earlier issue.

In Test 6, the best candidate (5.A) balanced viscosity for clean extrusion and achieved even white colonization. By adding cellulose, the biochar content was reduced, but this provided earlier access to a lignocellulose source. Shrinkage stayed in a low band (5–13%), but worse if compared with the most promising results from Test 4 (3–5%); and surfaces dried without skin cracking (Fig. 7).

Table 3 Compressive Strength and Elastic Modulus from preliminary uniaxial tests. Values for samples 1.1 and 3.3 are means of $N=4$ replicas (± standard deviation); values for samples 3.A-3.E correspond to a single specimen each ($N=1$) and are reported without standard deviation. Given the limited sample sizes, these values are indicative and do not support statistically significant comparisons across formulations

Sample	Diam. (mm)	Height (mm)	Cross Section (mm2)	Moisture Content (%)	N	Peak Force (N)	Stroke (mm)	Strain (%)	Compres. Strength (MPa)	Elastic Modulus (MPa)
1.1	50	50	1963	3	4	4175 ± 695	3.05 ± 0.75	5 ± 1	2.13 ± 0.35	37.11 ± 13.03
3.3	50	50	1963	3	4	2125 ± 299	4.68 ± 1.46	8 ± 2	1.08 ± 0.15	12.42 ± 4.29
3.A (G3)	60	120	2748	1	1	2000	6.60	6	0.8	14.46
3.A (G7)	60	120	2827	2	1	1900	5.20	4	0.66	15.37
3.B (G3)	60	120	2748	1	1	3100	7.80	6	1.24	19.2
3.B (G7)	60	120	2827	3	1	2900	6.00	5	1.16	23.16
3.C (G3)	60	120	2748	2	1	2400	7.20	6	0.96	15.91
3.D (G3)	60	120	2748	2	1	3500	6.00	5	1.45	28.9
3.D (G7)	60	120	2827	3	1	3700	7.00	6	1.41	24.48
3.E (G7)	60	120	2827	5	1	5000	9.00	8	1.91	25.53

To contextualize these values, Elsacker et al. (2019) reported shrinkage ranging from 9 to 20% across different lignocellulosic substrates. Aiduang et al. (2024) compiled a broader range of 2.78–17%, with bamboo sawdust substrates achieving 3.14–5.83%, the closest analogue to our specimens' values (3–5%). The shrinkage-mitigating role of biochar has been well documented in cementitious materials: Gupta et al. (2020) reported a 61% reduction in autogenous shrinkage and a 23% reduction in drying shrinkage when 5 wt% biochar replaced silica fume in cement mortar, attributing the effect to biochar's porous structure acting as an internal water reservoir. Our results suggest that an analogous mechanism may operate in mycelium composites, where biochar's capillary network moderates the rate of moisture loss during both incubation and drying.

When cellulose was added in Test 6, the increase to 5–13% shrinkage brought values closer to the conventional lignocellulosic MBC range, suggesting that the cellulose ratio is a primary driver of dimensional changes. The cellulose-rich blend (5.B) appears to allow faster initial hyphal development, forming a thicker white skin within days. However, the same substrate slowed water release and kept the bulk softer for longer, which manifested as slight edge rounding by the end of the first week. At the opposite extreme, the biochar-rich blend (5.C) dried in a crisp, geometrically accurate sample and preserved corners, but the surface coverage was thinner, and brittleness appeared especially at the center. Between these poles, the balanced ratio delivered the most robust performance for scaling (5.A): fast enough colonization for handling, sufficient cohesion to resist cracking when lifted, and visibly low warp. While cellulose is more easily degradable by the fungi, compared to biochar and wood fibers, mixes in Test 6 (5.A, 5.B, and 5.C) have more water, potentially reducing gas exchange needed for oxygenation. This is similar to what Soh et al. (2023) observed when higher agar concentrations improved shape fidelity but reduced mycelial colonization. The trade-off between structural and biological performance appears to be a common challenge across different MBC formulations. Because Test 7 would stress the fresh-state material with longer unsupported paths and challenging curvature, the composition that balanced better dimensional stability and biological process was prioritized over any composition that maximized a single attribute.

5.2 Reaction–diffusion toolpaths and biological and mechanical performances

Research question (b) asked whether reaction–diffusion-inspired toolpaths can balance oxygenation for mycelium growth with structural integrity during and after drying. Macroscopic observations across specimens and demonstrator-scale experiments suggest that the biomimetic toolpath logic generates two regions with visibly different surface behavior: open-porosity areas where aerial mycelium develops (*oxygen corridors*) and higher-overlap areas of denser, more cohesive material (*densification belts*). We adopt these terms as hypothesized architectural features based on macroscopic visual observation of surface colonization, since we did not perform finite element analysis to map stress distributions, or collect oxygen-sensor or porosity-gradient data. Accordingly, we do not claim that the toolpath produces a functionally graded material in

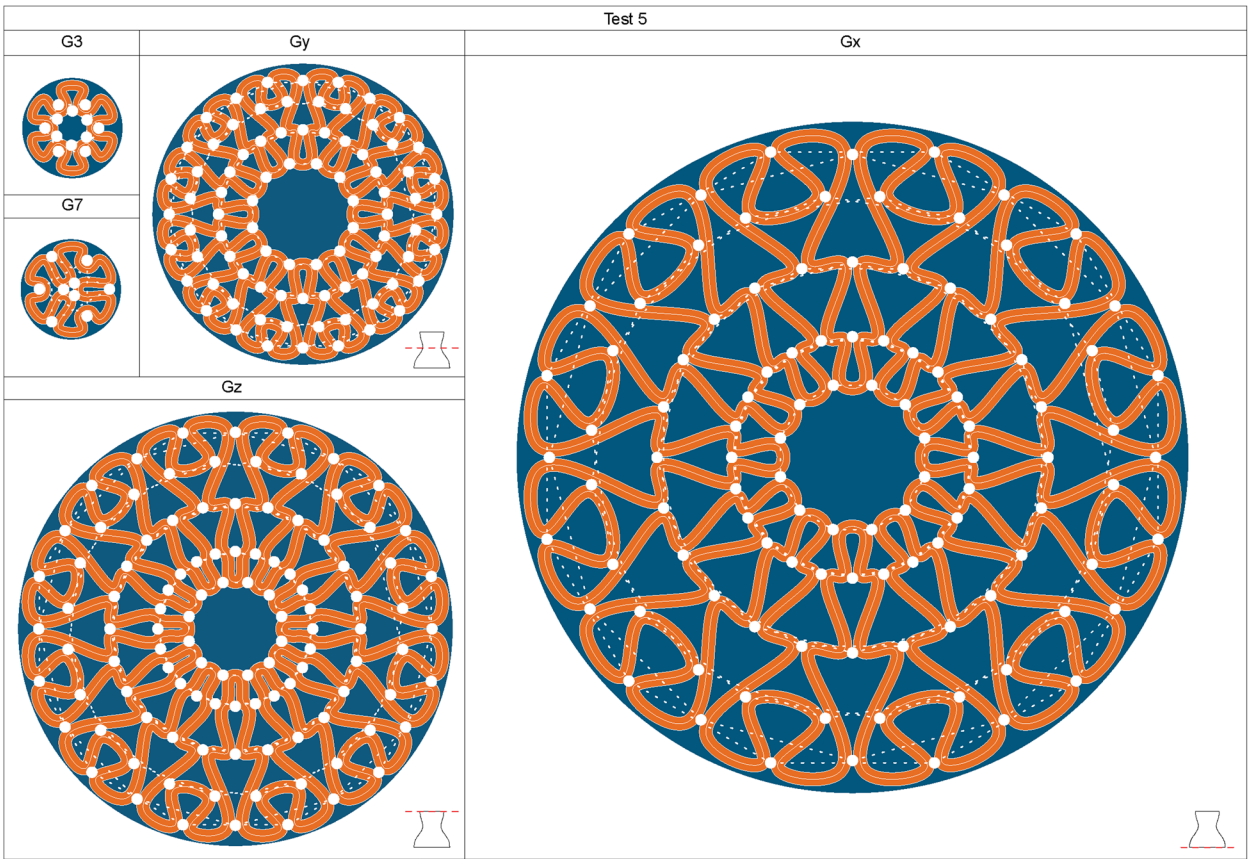

Sample	G3	G7	Gx	Gy	Gz
Z heigth	-	-	0 mm	230 mm	400 mm
Outer diameter	60 mm	60 mm	400 mm	194 mm	259 mm
Points clouds (rings)	2	3	5	4	5
Nozzle	6 mm	6 mm	8 mm	8 mm	8 mm
Merging points (M)	12	9	120	84	120
Porosity (φ_open)	52%	44%	59%	43 %	46%
Central cavity diameter	17 mm	-	83 mm	68 mm	58 mm

Fig. 6 Reaction–diffusion-inspired toolpaths evaluated from specimen to larger areas. The labels show *merging points* (M), *porosity* (Φ_open) and *densification belts*

the strict mechanical sense; the functional roles attributed to these regions remain to be verified in future work.

A biomimetic approach was adopted for the geometric exploration in Test 3: the reaction–diffusion pattern, a morphogenetic mechanism formalized by Alan Turing (1952) to explain how interacting substances that react locally and diffuse spatially can spontaneously generate stable patterns such as spots, stripes, and labyrinths (Fig. 4). The reaction–diffusion patterns observable in brain corals, known for facilitating effective fluid circulation and nutrient exchange, were chosen (Kaandorp, 1999). As demonstrated in previous studies, adequate oxygenation within mycelium composites enables more consistent mycelial growth (Aiduang et al., 2024). The hypothesis behind this approach is that if the extruded material remains sufficiently interconnected, it may maintain buildability while also providing adequate porosity for optimal aeration.

In Test 3, Geometry G3 seems to enable better oxygenation and mycelial growth compared to Geometry G7, maybe due to the addition of a continuous central cavity in the center of the sample that potentially acted as an *oxygen corridor*. Visual observation of results in Test 4 suggests that the integration of sawdust may have influenced mycelium development. The specimens showing more consistent mycelium development and dimensional stability (sample 3.A and 3.B with geometry G3) showed a shrinkage of 3–5% in the Z direction, measured through photographic analysis. Overall, over extruding the composite during layer deposition, approximately 1–2 mm more than the nozzle size, by setting the flow rate at 50–60%, and lowering the printing speed, with a

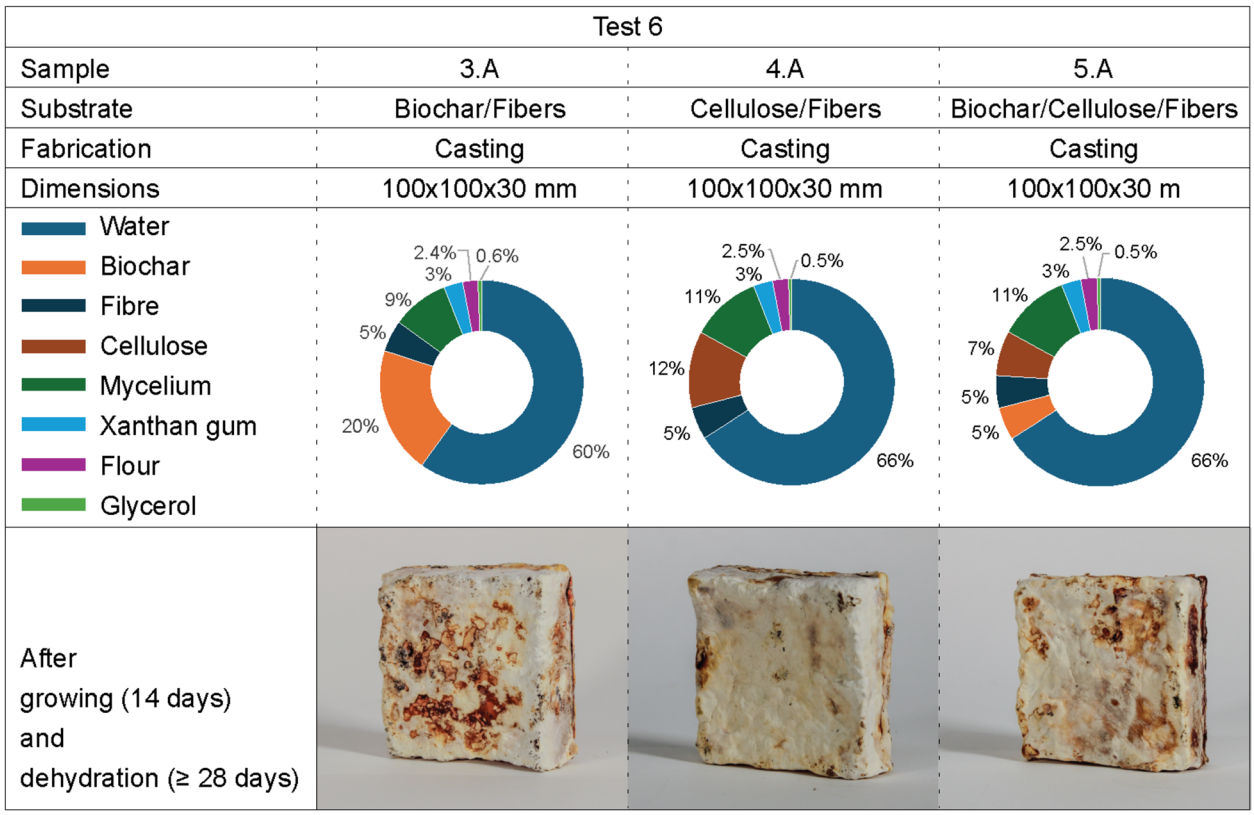

Fig. 7 Test 6 samples composition, fabrication method, and growing documentation after 14 days

feed rate at 40%–50%, led to better results in all the samples in Test 4.

Moreover, preliminary mechanical performance assessments on the samples showed compressive strength values between 0.66 MPa and 2.13 MPa, and elastic modulus values ranging from 12.42 MPa to 37.11 MPa (Table 3). Notably, formulations 3.A-E displayed comparable values and a progressive, foam-like compressive behavior without brittle fracture (Fig. 9-a). While groups 1.1 and 3.3 exhibited variability among 4 replicas of each, linked to issues in shrinkage, printing consistency, and uneven mycelial colonization. Preliminary compressive tests showed a trend of potential improvement in compressive strength and elastic modulus relative to values reported in the literature for other MBCs (Fig. 9-b). However, the limited sample size ($N=4$ replicas for samples 1.1 and 3.3, and $N=1$ for each of samples 3.A-3.E) does not support statistically significant conclusions, and these results should be read as preliminary indications motivating a more systematic mechanical analysis.

As shown in specimens in Set 1, the *foam-like* compressive response suggests that continuous paths and many short bridges act as micro-ribs that dissipate energy through sequential collapse, without single crack propagation (Fig. 9-a); this is consistent with our qualitative impression that a higher number of merging points helps to stabilize load transfer between adjacent strands while porosity maintains aeration for growth.

When moved to the larger demonstrator in Set 2, the same logic reads at a different scale: the *densification belts* behave as a connectivity skeleton that appears to preserve continuity across layers and, later, across the seam; the *oxygen corridors* seem to promote aerial hyphae and, during drying, accelerate moisture release. In these experiments, the toolpath design appeared, on visual inspection, to produce regions with distinguishable surface and porosity characteristics that we hypothesize correspond to different functional roles in load transfer and oxygen exchange. The observed behavior was not fully consistent across the demonstrator, and confirming this hypothesis will require dedicated structural simulation and instrumented monitoring.

Moving now to discuss results from Test 5, Fig. 6 shows the printing toolpath designed with the intention of distributing oxygenation and stability across the element. Visually, regions with higher relative humidity (*moisture wells*) appeared to support denser surface colonization, while regions with more open porosity

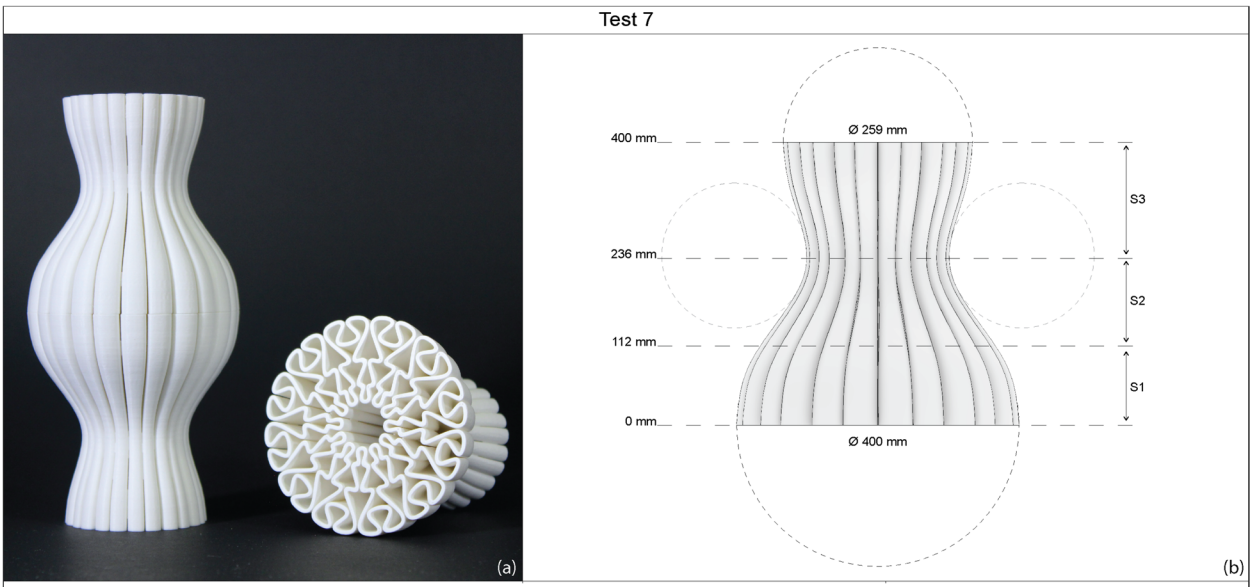

3D Printing parameters (d)

	Speed	Flow	Feed	Layer heigth	Nozzle	Overhang	Z - Day 0	Z - Day 14	Difference	Z - Day 28	Difference	Total Difference
S1	1200 mm/min	100%	100%	4 mm	8 mm	45 °	112 mm	95 mm	15%	87 mm	8%	22%
S2							124 mm	115 mm	7%	100 mm	13%	19%
S3							164 mm	135 mm	11%	138 mm	5%	15%

Fig. 8 **a** The top left image shows 1:5 prints validating the double-curved profile. **b** The top right drawings illustrate dimensions and overhang ≤ 45°. **c** The central images show grown prototypes (S1, S2, S3) exhibiting uniform surface colonization. **d** The bottom table summarizes printing parameters

(*oxygen corridors*) appeared to support aerial mycelial development. These macroscopic observations are consistent with the design intent of the pattern, though they do not constitute physical evidence of functional grading, yet. Sections at base/waist/top verified *oxygen corridors* and *moisture wells*, checking that diffusion distances and localized humidity remained in the same functional regime as at small-scale samples (Fig. 10). In Test 7, each segment printed cleanly and grew 14 days at 24 °C; dimensional checks showed low shrinkage along the Z axis but relevant collapsing; no contamination was observable in the fresh-state window. Surfaces exhibited uniform colonization across ridges and into wells, consistent with the designed *oxygen corridors*. Figure 8-c reports the height of the samples right after printing, after 14 days of incubation, and after drying, revealing total deformations of 22%, 19%, and 15%, respectively. We noticed that in the segments that experienced less collapsing (S2, S3): the porosity of the *oxygen corridors* promoted the development of aerial mycelium, which provided a foam-like mycelium envelope that could enhance thermal and acoustic insulation properties. On the other hand, the presence of *moisture wells* into the *densification belts,* shaped solid interconnections of the

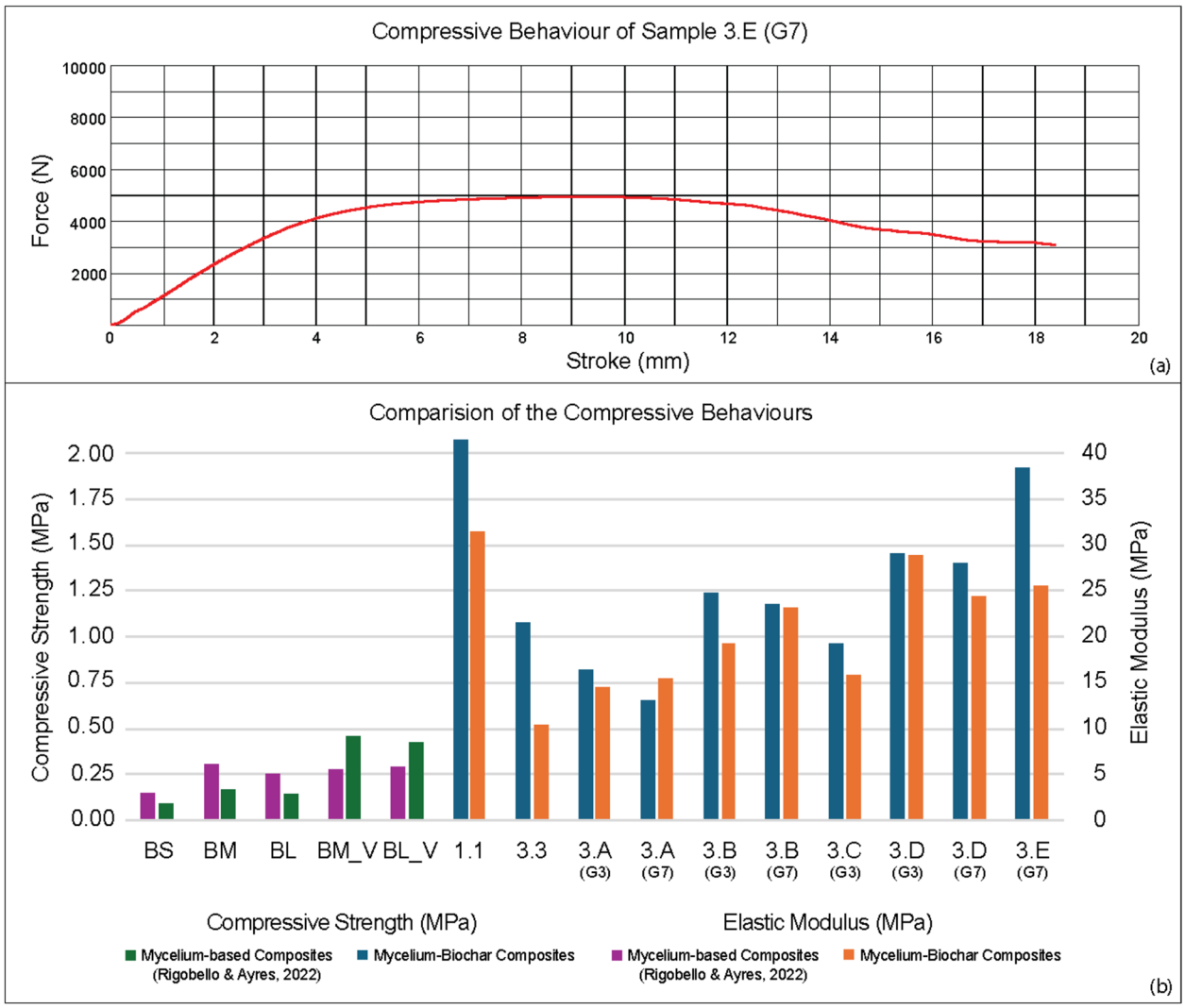

Fig. 9 **a** Sample 3.E (G7). Diagram displaying peak force (N) and compressive behavior during the stress test. **b** Compressive behaviors of mycelium-biochar compared to other mycelium-based composites. Samples 1.1 and 3.3 are the average of 4 replicas; samples 3.A-3.E are single-specimen measurements and are reported as indicative

material among the 3D printed layers, as shown in the sections analysis in Fig. 8-b. This might suggest that the composite living nature responded positively to the stimulation aimed during the design phase of the pattern.

The reaction–diffusion-inspired toolpaths and the way we tuned the density of the *merging points* and *porosity* provided a functional analogue to stress-driven rib networks. While our geometry was not computed from principal moment fields, the design logic, prioritizing path continuity and distributing material where continuity is structurally and biologically beneficial, parallels the anisotropic reaction–diffusion approach introduced by Zomparelli and Naboni (2023), where a reaction–diffusion system is driven by principal stresses/moments to generate isostatic, maze-like rib patterns whose density and thickness can be locally tuned. In our tests, densifying merging points increased continuous load paths across the print while maintaining aeration and moisture management. Conceptually, this mirrors the isostatic reaction–diffusion framework except that our optimization focuses on fabrication constraints and biological performance, not on finite-element principal moments.

More directly, Gomaa et al. (2024) provided the first quantitative dataset linking geometric parameters (infill density, internal walls, bracing patterns) to mycelium growth rates and mechanical performance in 3D-printed MBCs, establishing that geometry may contribute to design the biological behavior.

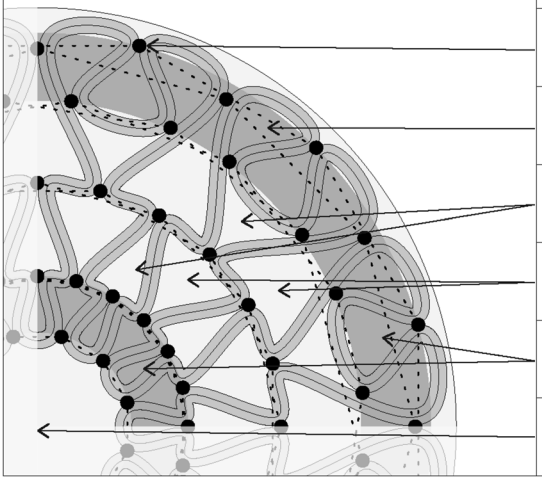

Functions of the Geometry		
Type	Purpose	Description
Merging points (M)	*Structural*	In these points the path blends to itself during the extrusion
Point clouds (Rings)	*Structural*	Groups of points that weave to generate the relative ring patterns
Moisture Wells	*Porosity (Φ_open)*	Smaller areas that keep higher moisture and grow harder mycelium
Oxygen Corridors	*Porosity (Φ_open)*	Areas with higher porosity that promote softer aereal mycelium
Densification Belts	*Structural*	Close rings that shape only moisture wells to provide stiffness
Central Cavity	*Porosity (Φ_open)*	Central hollows that allow airflows for dring the elements

Fig. 10 Different parts of the pattern have different functions; the tab explains the characteristics of this graded structure

Our reaction–diffusion-inspired toolpath sits within this same conceptual frame, although we did not parametrize the growth-geometry coupling at a data-driven level.

5.3 Upscaling, bio-welding, and dimensional stability at demonstrator scale

Research question (c) asked whether the design and material insights from the Experimental Set 1 could be upscaled, and as a related question, whether dried 3D-printed parts could be reactivated and bio-welded into a continuous element while maintaining structural integrity. The 3D printing and bio-welding performed in Tests 7 and 8 produced a single element with visually continuous seams and uniform surface colonization, though dimensional stability connected to the fresh-state window remains a challenge requiring further investigation.

The second experimental set translated the material and geometric rules from the specimen to a larger demonstrator of 400 mm diameter and 400 mm height. Splitting the demonstrator into 3 segments along the Z axis (S1-S3) reduced the risk of collapsing during the wet state window. Each segment was printed cleanly, colonized uniformly in 14 days, and was bio-welded for 7 days. However, maintaining dimensional stability during the scale-up was challenging. Specifically, balancing water content against self-weight remained difficult during late colonization and especially at assembly, when partially dried segments still carried enough mass to bias the profile. Figure 11 documents this process.

The most direct existing precedent for the bio-welded assembly logic explored here is Modanloo et al.'s (2021) *Tilted Arch*, in which individually 3D-printed MBC blocks were assembled into a tilted-arch geometry and

Fig. 11 Process timeline for the demonstrator: **a** freshly printed composite with reaction–diffusion toolpaths; **b** segments positioned after colonization over 14 days; **c** 7 days after, the elements are welded together biologically, ready for final drying, after which the piece behaves as a single element; **d** 28 days after, the connections are solid, being dried at room temperature to keep self-healing properties

co-incubated, with hyphae bridging the inter-block interfaces. Their adoption of a compression-only catenary geometry to compensate for low material stiffness frames the same design logic our segmented demonstrator pursues at a larger scale.

Abdallah and Estévez (2023) documented how Pleurotus ostreatus hyphae infiltrate and bridge between 3D printed lattice profiles, with the strongest bio-welding detected at corners and lateral zones where curvature amplifies interface exposure; Scanning Electron Microscopy (SEM) showed dense hyphal networks spanning layer interfaces and fixing the joint. Although this study does not include SEM analysis, a visual examination suggests that our *oxygen corridors* and *moisture wells* echo this principle: by preserving porosity at the interface, ensuring contact between colonized faces, and through the application of a thin layer of fresh paste, we set the conditions that support hyphal penetration and bridging across the seam.

After the biological welding of the seams in Test 8, to evaluate how the scaled demonstrator performed after printing, incubation, and drying, the height of each segment (S1-S3) was monitored at 3 key stages, and the digital design was overlapped with a sectioned view of the manufactured segments for visual comparison. Digital sections of the toolpaths alongside physical cross-sections illustrate that the geometry preserved material continuity across the seam; the overall profile, however, was not preserved, since the demonstrator collapsed progressively under self-weight during the wet state and continued to deform during drying. Figure 12 shows how the demonstrator changes when compared to the digital model in 3 specific sections. This analysis checked if the considerations made during the design phase were effective in shaping *oxygen corridors*, *moisture wells,* and *densification* belts, resulting in a graded structure. With these sections, the dimensional changes caused by the collapsing of the material and shrinkage during the drying phase are observable as well.

Moreover, Elsacker et al. (2023) showed that pure mycelium materials can express self-healing after damage via biological revival (with chlamydospores, present in strains like *Ganoderma lucidum* M9726), recovering mechanical performance after short reactivation periods

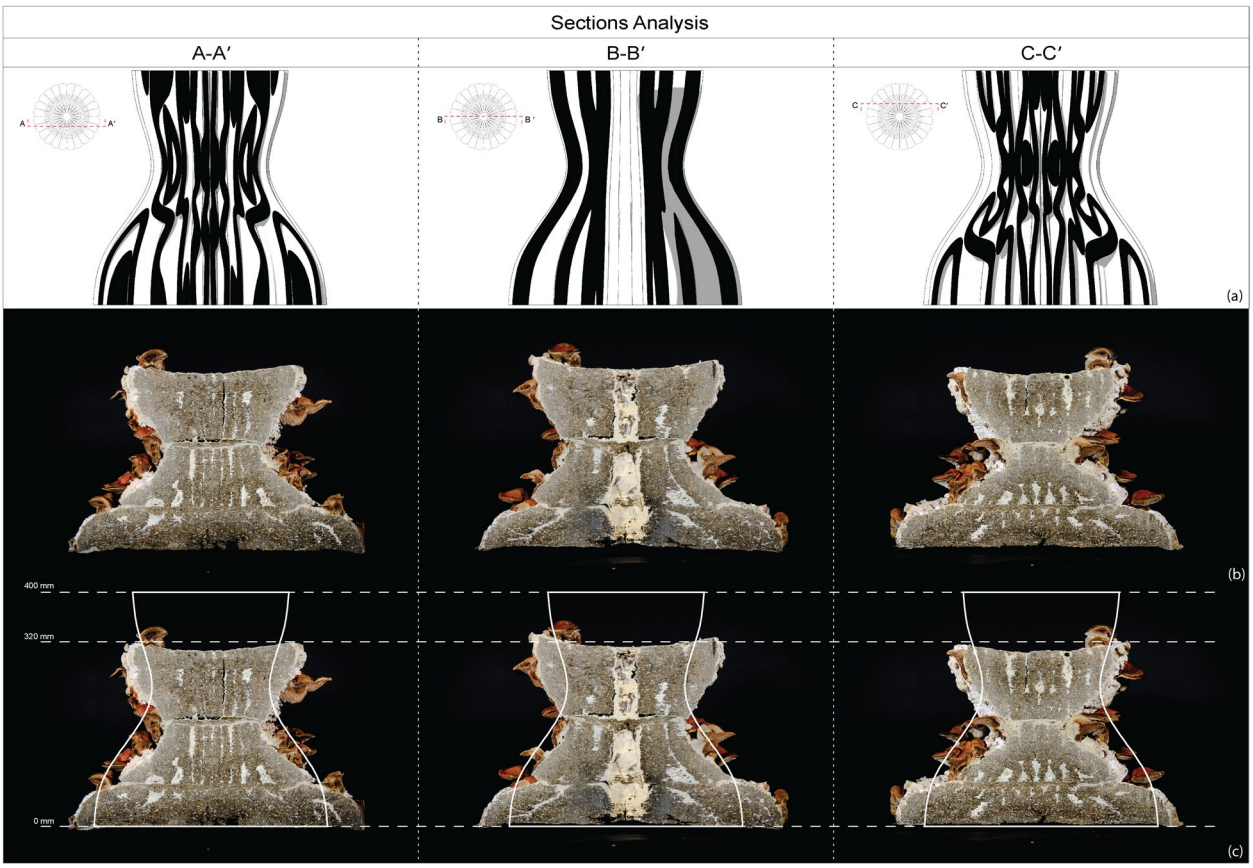

Fig. 12 **a** Digital sections of the geometry showing the intended cavities and profile. **b** Physical cross-sections of the 3D printed and bio-welded demonstrator. **c** Comparison of the dimensional stability between the design and the element

even from dry, oligotrophic states. Our choice to air-dry and avoid drying through heat is consistent with keeping the seam biologically reactivatable; together with the weld continuity and fruiting we observed, this supports positioning our assembly protocol as a bio-welding that can, in principle, be locally reactivated for repair or re-joining. The resulting artifact, free of visible contamination and exhibiting localized fruiting bodies, illustrates both the feasibility and the current limits of this building method; the outcome is shown in Fig. 13.

6 Potential implications for architecture

6.1 Structural logic and aesthetics

Although the preliminary mechanical tests do not yet support statistically significant conclusions, the foam-like compressive response visible in Fig. 9-a, together with the low tensile capacity typical of MBCs, tentatively suggests biochar-mycelium composites as candidate materials for lightweight, compression-dominated structural elements such as shells, vaults, and domes. This suggests using MBCs in monolithic, biomimetic geometries that are self-supporting through their curvature and an internal porosity distribution shaped to integrate biological and structural functions. It should be noted that the compressive strengths reported here, like those across the 3D-printed MBC literature, remain two to three orders of magnitude below those of structural concrete and well below the 17 MPa floor typically required for low-density structural applications. The shell-and-vault applications discussed here are therefore credible only in conjunction with rigorous form-finding to keep all stresses compressive and remain contingent on geometric efficiency rather than absolute material capacity. On the other hand, MBCs have biological implications that might impact their perception. For example, the white mycelial skin that forms during incubation, the localized fruiting bodies observed during drying (Fig. 13), and the potential for re-colonization after reactivation could evolve over short periods of time, producing variable surface finish, color, and texture. These conditions follow the contemporary discourse around the transformational quality of biobased materials in time and process (Thomsen & Tamke, 2022).

6.2 Prefabrication, assembly, and durability

The prefabrication and bio-welding workflow explored in this work outlines a fabrication logic analogous to bricks and mortar: elements are printed, grown, dried, and stored as inert stock, then joined on site with a thin bed of moist composite that triggers biological reactivation during a short, allowed window. This logic decouples fabrication from assembly and allows components to be manufactured in controlled laboratory or workshop conditions, transported dry, and assembled with minimal on-site infrastructure. For architecture, this could mean that complex and lightweight geometries produced with MBC can be decomposed into printable segments whose interfaces are geometrically encoded for positional tolerance, reducing the precision demands on-site.

However, this biological potential also imposes constraints: components must be protected from uncontrolled moisture exposure, which could trigger unwanted growth or contamination, and they must be shielded from sustained outdoor weathering until long-term durability protocols are established. These constraints also limit the most promising applications to interior partitions, insulation panels, acoustic elements, and protected envelope components. Sharma and Le Ferrand (Sharma et al., 2026) recently reported the first quantitative service-life specification for 3D-printed MBCs, with degradation half-lives of 53.47 days (wood-PLA matrix) and 143.94 days (wood-PCL matrix) under cyclic dry-sun-rain exposure, suggesting that degradation can be reframed as a tunable design parameter.

Fig. 13 Demonstrator after more than 28 days of air drying, fruiting bodies emerged: no visible contamination

6.3 Circularity and societal impact

The biochar used in this study comes from Swedish biogas production residues, the sawdust is collected from the university wood shop, the cellulose is extracted from recycled cardboard from packaging and deliveries in the lab, and the fungal organism itself can be cultivated everywhere. Unlike materials that depend on global supply chains and energy-intensive processing, this composite can, in principle, be formulated from regionally available waste streams, linking construction directly to local production flows. At the end of life, the composite is biodegradable, and its biochar content represents sequestered carbon that would otherwise return to the atmosphere, enabling buildings to function as temporary carbon sinks. This positions the material within a regenerative construction paradigm where resource extraction, use, and return are perceived as a continuous cycle (Alemu et al., 2022).

It must be acknowledged that these architectural implications are, at present, largely speculative. The mechanical values reported here are comparable to low-density foams and insulation boards, not structural timber or concrete; fire reaction, acoustic attenuation, and hygrothermal performance remain untested; and as far as the authors know, no building code currently recognizes MBC as a construction material. The path from laboratory prototypes to architectural applications requires not only further material characterization but also building-physics testing, regulatory engagement, and full Life Cycle Assessment. Nevertheless, the experimental results presented in this study, particularly the shrinkage control, the prefabrication through bio-welding, and the hypothesized functional grading through toolpath design, represent necessary preconditions for that translation and the architectural implications outlined above.

7 Conclusion

7.1 Contributions

This study set the stage for a practical process window for biochar-mycelium composites fabricated via LDM and suggests that reaction–diffusion-inspired toolpaths can simultaneously support (i) buildability during printing and (ii) biological activity relevant to prefabricated, modular components.

Three principal contributions emerge; each tied to a specific research question. Addressing RQ (a), biochar and mycelium were shown to be compatible in 3D printable composites; rice flour as a nutrient source seems to promote uniform colonization and contamination resistance under low-sterility conditions, while the biochar-cellulose-fiber formulation (5.A) delivered the most consistent combination of viscosity, colonization, and dimensional stability, among the ones tested in this study.

Addressing RQ (b), the biomimetic toolpath produced visually distinguishable regions across the printed elements, *oxygen corridors,* and *densification belts,* which, based on macroscopic observation, appeared to support, respectively, aerial mycelial development and buildability. These functional roles remain hypothesized rather than physically verified. Preliminary compressive tests showed a foam-like response, with vertical shrinkage as low as 3–5% in a subset of coupon-scale specimens; these values should be read as indicative under specific conditions.

Addressing RQ (c), the parametric upscaling from specimen to demonstrator scale showed that *merging points* density and *porosity* can be held constant across sections by scaling concentric point-cloud rings with constant ϕ. Segmentation into 3 printable parts and bio-welding with a thin layer of fresh paste produced visually continuous seams and uniform colonization, though dimensional stability during the fresh-state window remains a challenge that requires further investigation.

7.2 Limitations and future work

The study is bounded by a laboratory-scale workflow and a limited parameter space. Key material inputs were not fully characterized. Specifically, the biochar's feedstock and pyrolysis conditions, the workshop sawdust's wood species and prior treatments, and the wood-fiber pellets' lignin and cellulose composition remain unknown, which limits the strict reproducibility of the formulations reported here, since identical mass ratios would not necessarily yield identical biological or mechanical behavior with inputs of a different source. Mechanical testing was limited to uniaxial comparison of representative specimens, and environmental durability was not addressed. Future work will pursue characterization of the industrial by-products used, water content variation for dimensional stability in the wet state, and mechanical analysis to verify the 3D printed gradients' performance.

Acknowledgements

This manuscript is an extension of a CDRF paper entitled "Biobased Material Confluences: Investigating Material Formulation and 3D Printing Parameters for Biochar-Mycelium Building Composites" (Errichiello & Diarte Almada, 2025).

Authors' contributions

Raffaele Errichiello led conceptualization, methodology, investigation, data curation, visualization, and writing of the original draft. Julio C. Diarte Almada contributed to supervision, methodology, validation, and review and editing of the manuscript.

Funding

The work done in this study was possible thanks to funding from The JC Kempe Memorial Scholarship Foundation through the Umeå Student Union and material resources and equipment from the Material Practices Lab at Umeå School of Architecture acquired through the Faculty of Science and Technology at Umeå University.

Data availability
The underlying materials/images, printing parameters and files for the specimens, the demonstrator, and seam geometry are available from the corresponding author upon request.

Declarations

Ethics approval and consent to participate
Not applicable.

Consent for publication
Not applicable.

Competing interests
The authors declare no competing financial or personal interests.

Received: 6 November 2025 Revised: 20 May 2026 Accepted: 7 June 2026
Published online: 18 June 2026

References

Abdallah, Y. K., & Estévez, A. T. (2023). Biowelding 3D-printed biodigital brick of seashell-based biocomposite by *Pleurotus ostreatus* mycelium. *Biomimetics,8*(6), Article 504. https://doi.org/10.3390/biomimetics8060504

Aiduang, W., Jatuwong, K., Luangharn, T., Jinanukul, P., Thamjaree, W., Teeraphantuvat, T., Waroonkun, T., & Lumyong, S. (2024). A review delving into the factors influencing mycelium-based green composites (MBCs) production and their properties for long-term sustainability targets. *Biomimetics,9*(6), Article 337. https://doi.org/10.3390/biomimetics9060337

Alemu, D., Tafesse, M., & Mondal, A. (2022). Mycelium-based composite: The future sustainable biomaterial. *International Journal of Biomaterials*. https://doi.org/10.1155/2022/8401528

Baharlou, E. (2025). Nutrient-enriched soil inks for 3D-printed mycelium-based living building materials. *Materials & Design,259*, Article 114770. https://doi.org/10.1016/j.matdes.2025.114770

Bai, X. B., van Wijngaarden, E. W., Silberstein, M. N., & Wisniewska, M. H. (2025). Engineering shootable mycelium-bound composites (MBCs) as living building materials. *Materials Advances,6*(22), 8541–8557. https://doi.org/10.1039/D5MA00656B

Bhardwaj, A., Vasselli, J., Lucht, M., Pei, Z., Shaw, B., Grasley, Z., Wei, X., & Zou, N. (2020). 3D printing of biomass-fungi composite material: A preliminary study. *Manufacturing Letters,24*, 96–99. https://doi.org/10.1016/j.mfglet.2020.04.005

Chadha, K., Paoletti, I. M., Carcassi, O. B., & Ramos Montilla, N. (2023). Programmed Growth: A Living Mycelium and Clay Composite. *28th Interntional Conference of the Association for Computer-Aided Architectural Design Research in Asia (CAADRIA)*, *2*, 311–320. https://doi.org/10.52842/conf.caadria.2023.2.311.

Elsacker, E., Vandelook, S., Brancart, J., Peeters, E., & De Laet, L. (2019). Mechanical, physical and chemical characterisation of mycelium-based composites with different types of lignocellulosic substrates. *PLoS ONE*. https://doi.org/10.1371/journal.pone.0213954

Elsacker, E., Peeters, E., & De Laet, L. (2022). Large-scale robotic extrusion-based additive manufacturing with living mycelium materials. *Sustainable Futures,4*, Article 100085. https://doi.org/10.1016/j.sftr.2022.100085

Elsacker, E., Zhang, M., & Dade-Robertson, M. (2023). Fungal Engineered Living Materials: The Viability of Pure Mycelium Materials with Self-Healing Functionalities. *Advanced Functional Materials,33*(29), 2301875. https://doi.org/10.1002/adfm.202301875

Elsner, S., Jesch, R., Weisheit, L., Boxberger, L., Ihlenfeldt, S., & Drossel, W.-G. (2024). Development approach of a workflow for 3D printing of living mycelium materials and their growth manipulation. *Procedia CIRP,125*, 302–307. https://doi.org/10.1016/j.procir.2024.08.051

Errichiello, R., & Diarte Almada, J. (2025). Biobased Material Confluences: Investigating Material Formulation and 3D Printing Parameters for Biochar-Mycelium Building Composites. *7th International Conference on Computational Design and Robotic Fabrication (CDRF 2025): Transindividual Intelligence. ISBN 978-981-92-0614-8*

Ghazvinian, A., & Gürsoy, B. (2022). Mycelium-Based Composite Graded Materials: Assessing the Effects of Time and Substrate Mixture on Mechanical Properties. *Biomimetics,7*(2), 48. https://doi.org/10.3390/biomimetics7020048

Gomaa, H., Chau, W. M., Karazi, Y., Biala, E., Akbar, Z., Wortmann, T., & Ostermann, M. (2024). Influence of geometry on growth and strength of 3D-printed mycelium composites: A data-driven study. In P. Eversmann, C. Gengnagel, J. Lienhard, M. Ramsgaard Thomsen, & J. Wurm (Eds.), *Scalable disruptors* (pp. 331–345). Springer. https://doi.org/10.1007/978-3-031-68275-9_27

Gupta, S., Krishnan, P., Kashani, A., Kua, H. K., & Kua, H. W. (2020). Application of biochar from coconut and wood waste to reduce shrinkage and improve physical properties of silica fume-cement mortar. *Construction and Building Materials,262*, Article 120688. https://doi.org/10.1016/j.conbuildmat.2020.120688

Kaandorp, J. A. (1999). Morphological analysis of growth forms of branching marine sessile organisms along environmental gradients. *Marine Biology,134*(2), 295–306. https://doi.org/10.1007/s002270050547

Leschok, M., & Dillenburger, B. (2022). 3D Printed formwork for Mycelium Bound Composites. *42nd Annual Conference of the Association for Computer Aided Design in Architecture (ACADIA)*, (pp. 356–365). https://doi.org/10.52842/conf.acadia.2022.1.356

Madusanka, C., Udayanga, D., Nilmini, R., Rajapaksha, S., Hewawasam, C., Manamgoda, D., & Vasco-Correa, J. (2024). A review of recent advances in fungal mycelium based composites. *Discover Materials,4*(1), 13. https://doi.org/10.1007/s43939-024-00084-8

Modanloo, B., Ghazvinian, A., Matini, M. R., & Andaroodi, E. (2021). Tilted Arch; Implementation of Additive Manufacturing and Bio-Welding of Mycelium-Based Composites. *Biomimetics,6*(4), 68. https://doi.org/10.3390/biomimetics6040068

Mohanty, A. K., Vivekanandhan, S., Das, O., Romero Millán, L. M., Klinghoffer, N. B., Nzihou, A., & Misra, M. (2024). Biocarbon materials. *Nature Reviews Methods Primers,4*, Article 19. https://doi.org/10.1038/s43586-024-00297-4

Mohseni, A., Rocha Vieira, F., Pecchia, J. A., & Gürsoy, B. (2023). Three-Dimensional Printing of Living Mycelium-Based Composites: Material Compositions, Workflows, and Ways to Mitigate Contamination. *Biomimetics,8*(2), 257. https://doi.org/10.3390/biomimetics8020257

Özdemir, E., Saeidi, N., Javadian, A., Rossi, A., Nolte, N., Ren, S., Dwan, A., Acosta, I., Hebel, D. E., Wurm, J., & Eversmann, P. (2022). Wood-Veneer-Reinforced Mycelium Composites for Sustainable Building Components. *Biomimetics,7*(2), 39. https://doi.org/10.3390/biomimetics7020039

Özdemir, E., Rossi, A., & Eversmann, P. (2025). MycoCurva: Stay-in-place fabric formworks for curved veneer-reinforced mycelium building components. *Architecture, Structures and Construction,5*(1), 16. https://doi.org/10.1007/s44150-025-00134-6

Panjalipoursangari, N., Ou, Y., Schmidt, B., Müller, W. H., & Völlmecke, C. (2025). Impact of Fomes fomentarius growth on the mechanical properties of material extrusion additively manufactured PLA and PLA/Hemp biopolymers. *Fungal Biology and Biotechnology,12*(1), 14. https://doi.org/10.1186/s40694-025-00205-9

Rigobello, A., & Ayres, P. (2022). Compressive behaviour of anisotropic mycelium-based composites. *Scientific Reports,12*(1), 6846. https://doi.org/10.1038/s41598-022-10930-5

Rossi, A., Javadian, A., Acosta, I., Özdemir, E., Nolte, N., Saeidi, N., Dwan, A., Ren, S., Vries, L., Hebel, D. E., Wurm, J., & Eversmann, P. (2022). HOME: Wood-Mycelium Composites for CO 2 -Neutral, Circular Interior Construction and Fittings. *IOP Conference Series: Earth and Environmental Science,1078*(1), Article 012068. https://doi.org/10.1088/1755-1315/1078/1/012068

Schyck, S., Marchese, P., Amani, M., Ablonczy, M., Spoelstra, L., Jones, M., Bathaei, Y., Bismarck, A., & Masania, K. (2024). Harnessing fungi signaling in living composites. *Global Challenges,8*(8), Article 2400104. https://doi.org/10.1002/gch2.202400104

Sharma, R., & Sumbria, R. (2022). Mycelium bricks and composites for sustainable construction industry: A state-of-the-art review. *Innovative Infrastructure Solutions,7*(5), 298. https://doi.org/10.1007/s41062-022-00903-y

Sharma, D., Tan, J. J. R., & Le Ferrand, H. (2026). Living wood-polymer composites with tunable half-lives and enhanced performance. *Advanced Sustainable Systems,10*(1), Article e01446. https://doi.org/10.1002/adsu.202501446

Shen, S. C., Lee, N. A., Lockett, W. J., Acuil, A. D., Gazdus, H. B., Spitzer, B. N., & Buehler, M. J. (2024). Robust myco-composites: A biocomposite platform for versatile hybrid-living materials. *Materials Horizons,11*(7), 1689–1703. https://doi.org/10.1039/D3MH01277H

Soh, E., Teoh, J. H., Leong, B., Xing, T., & Le Ferrand, H. (2023). 3D printing of mycelium engineered living materials using a waste-based ink and non-sterile conditions. *Materials & Design,236*, Article 112481. https://doi.org/10.1016/j.matdes.2023.112481

Thomsen, M. R., & Tamke, M. (2022). Towards a transformational eco-metabolistic bio-based design framework in architecture. *Bioinspiration & Biomimetics*. https://doi.org/10.1088/1748-3190/ac62e2

Turing, A. M. (1952). The chemical basis of morphogenesis. *Philosophical Transactions of the Royal Society of London. Series B, Biological Sciences,237*(641), 37–72. https://doi.org/10.1098/rstb.1952.0012

Wang, D., Jantwal, A., Kaynak, E., Sas, G., & Das, O. (2025). Promoting internal curing in concrete by replacing sand with sustainable biochar. *Case Studies in Construction Materials,22*, Article e04542. https://doi.org/10.1016/j.cscm.2025.e04542

Zhang, Y., Li, M., Zhu, X., Wang, L., Mašek, O., Sarmah, A. K., & Tsang, D. C. (2025). Enhanced thermal insulation of biochar-gypsum composites. *Cement and Concrete Composites,159*, Article 106013. https://doi.org/10.1016/j.cemconcomp.2025.106013

Zomparelli, A., & Naboni, R. (2023). Generative design of isostatic ribbed slabs using anisotropic Reaction-Diffusion. *International Association for Shell and Spatial Structures IASS 2023: Digital modelling and fabrication*, (pp. 1–12). Melbourne. ISBN 978-064-68-7830-0

Publisher's Note